MAGICC haloes: confronting simulations with observations of the circumgalactic medium at $z = 0$

G. S. Stinson,[1]⋆ C. Brook,[2,3] J. Xavier Prochaska,[1,4] Joe Hennawi,[1] Sijing Shen,[4] J. Wadsley,[5] Andrew Pontzen,[6] H. M. P. Couchman,[5] T. Quinn,[7] Andrea V. Macciò[1] and Brad K. Gibson[2,8]

[1]*Max-Planck-Institut für Astronomie, Königstuhl 17, 69117, Heidelberg, Germany*
[2]*Jeremiah Horrocks Institute, University of Central Lancashire, Preston PR1 2HE*
[3]*Departamento de Física Teórica, Universidad Autónoma de Madrid, E-28049 Cantoblanco, Madrid, Spain*
[4]*Department of Astronomy & Astrophysics, UCO/Lick Observatory, University of California, 1156 High St, Santa Cruz, CA 95064, USA*
[5]*Department of Physics and Astronomy, McMaster University, Hamilton, Ontario L8S 4M1, Canada*
[6]*Sub-Department of Astrophysics, University of Oxford, Denys Wilkinson Building, Keble Road, Oxford OX1 3RH*
[7]*Astronomy Department, University of Washington, Box 351580, Seattle, WA 98195-1580, USA*
[8]*Department of Astronomy & Physics, Saint Mary's University, Halifax, Nova Scotia B3H 3C3, Canada*

ABSTRACT

We explore the circumgalactic medium (CGM) of two simulated star-forming galaxies with luminosities $L \approx 0.1$ and $1\,L^\star$ generated using the smooth particle hydrodynamic code GASOLINE. These simulations are part of the Making Galaxies In a Cosmological Context (MAGICC) program in which the stellar feedback is tuned to match the stellar mass–halo mass relationship. For comparison, each galaxy was also simulated using a 'lower feedback' (LF) model which has strength comparable to other implementations in the literature. The 'MAGICC feedback' (MF) model has a higher incidence of massive stars and an approximately two times higher energy input per supernova. Apart from the low-mass halo using LF, each galaxy exhibits a metal-enriched CGM that extends to approximately the virial radius. A significant fraction of this gas has been heated in supernova explosions in the disc and subsequently ejected into the CGM where it is predicted to give rise to substantial O VI absorption. The simulations do not yet address the question of what happens to the O VI when the galaxies stop forming stars. Our models also predict a reservoir of cool H I clouds that show strong Lyα absorption to several hundred kpc. Comparing these models to recent surveys with the *Hubble Space Telescope*, we find that only the MF models have sufficient O VI and H I gas in the CGM to reproduce the observed distributions. In separate analyses, these same MF models also show better agreement with other galaxy observables (e.g. rotation curves, surface brightness profiles and H I gas distribution). We infer that the CGM is the dominant reservoir of baryons for galaxy haloes.

Key words: methods: miscellaneous – galaxies: evolution – intergalactic medium.

1 INTRODUCTION

In the paradigm of cold dark matter cosmology, gravitational collapse leads to the formation of virialized and bound dark matter haloes. It is predicted that baryons fall into these haloes with the dark matter, comprising a mass fraction up to the cosmological ratio. Recent analyses indicate that stars comprise less than 25 per cent of the baryons that should have collapsed into haloes (Conroy

& Wechsler 2009; Mandelbaum et al. 2009; Guo et al. 2010; Moster et al. 2010; More et al. 2011). This presents a 'missing baryon' problem reflected in the unknown whereabouts of the baryons, which did not cool to form stars. Substantial amount of gas is found in a diffuse and highly ionized medium which is referred to as halo gas or the circumgalactic medium (CGM).

The CGM is known to manifest in at least two phases: (i) a warm/hot, collisionally ionized gas with temperature near the virial temperature ($T \gtrsim 10^6$ K) and (ii) a cooler phase (perhaps predominantly photoionized) with temperature $T \lesssim 10^4$ K. The latter phase has been detected in 21 cm emission in our Galaxy in the population

⋆ E-mail: stinsongr@gmail.com

known as the high-velocity clouds (e.g. Wakker & van Woerden 1997) lying at distances of tens of kpc (Thom et al. 2006). The hotter phase may be observed via bremsstrahlung emission with X-ray telescopes, in the intracluster medium of massive galaxy clusters (e.g. Allen, Schmidt & Fabian 2001), but so far extended diffuse emission has only been detected around one disc galaxy, the massive NGC 1961 (Anderson & Bregman 2011). Smaller disc galaxies have X-ray bright outflows (Strickland et al. 2004), but halo emission remains undetected.

The diffuse nature of the CGM makes positive detections of emission rare. The majority of empirical constraints, therefore, come from the absorption-line analysis of galactic haloes, along coincident sightlines to distant quasars and galaxies (e.g. Lanzetta, Wolfe & Turnshek 1995; Bowen, Blades & Pettini 1996; Chen & Tinker 2008; Rubin et al. 2010; Steidel et al. 2010). These observations reveal a cool and frequently metal-enriched phase traced by H I Lyman series absorption (e.g. Chen & Lanzetta 2003) and low-ionization metal-line transitions (e.g. Chen & Tinker 2008; Barton & Cooke 2009; Rubin et al. 2012). Importantly, galaxies of essentially all luminosity and spectral type exhibit significant H I absorption out to impact parameters $R \approx 300$ kpc (Wakker & Savage 2009; Prochaska et al. 2011b), implying a massive ($M \sim 10^{10}$ M$_\odot$) extended CGM.

A particularly useful tracer of the hot phase in quasar absorption-line analysis is the O VI doublet, which occurs in highly ionized and enriched regions of the Universe. If collisionally ionized, the gas has temperature $T \sim 10^5$–10^6 K. O VI is observed along the majority of sightlines through our Galactic halo and is believed to trace coronal material on scales of 10–100 kpc (Sembach et al. 2003). This gas is also associated with the CGM of local $L > 0.1 L^\star$ galaxies (Stocke et al. 2006; Wakker & Savage 2009). Prochaska et al. (2011b) have further demonstrated that the extended CGM ($R \sim 300$ kpc) of $L \gtrsim 0.1 L^\star$ galaxies has a high covering fraction to O VI and can account for all of the O VI detected in the present-day universe. Most recently, Tumlinson et al. (2011) have reported a nearly 100 per cent incidence of strong O VI absorption for the haloes of $L \sim L^\star$ star-forming galaxies, with an ionized metal mass that likely exceeds that of the galaxies' interstellar media, demonstrating that the CGM is a major reservoir of highly ionized metals at $z \sim 0$.

The observations reveal a multiphase, highly ionized and metal-enriched CGM around present-day galaxies (also see Thom & Chen 2008b; Savage, Lehner & Narayanan 2011a; Savage et al. 2011b; Wakker et al. 2012). The high degree of enrichment demands that a large mass of gas (and metals) is transported from galaxies and/or their progenitors to the CGM. Thus, these observations provide robust constraints on the processes of gas accretion and feedback which may be compared directly against models of galaxy formation.

Previous theoretical work on the CGM for individual galaxies has largely focused on analytic or semi-analytic treatments of idealized gas and dark matter/temperature profiles (Mo & Miralda-Escude 1996; Telfer et al. 2002; Maller & Bullock 2004; Binney, Nipoti & Fraternali 2009). Although these works provide crucial insight into the nature of the CGM, they lack proper cosmological context (e.g. mergers) and have generally not included the role of feedback from star formation in the galaxy and its satellites. The latter is now considered critical to match a wide range of galaxy observables including the luminosity function, the stellar mass–halo mass relationship and the baryonic Tully–Fisher relationship (Guo et al. 2011). Galactic-scale winds likely resulting from stellar feedback are a nearly generic feature of star-forming galaxies (Shapley et al. 2003; Weiner et al. 2009; Rubin et al. 2010) and may significantly influence the properties of the CGM.

A number of groups have now used cosmological simulations to examine the nature and enrichment of the IGM at $z \sim 0$ and offer comparisons to quasar absorption-line observations (e.g. Cen & Ostriker 2006; Cen 2010; Davé et al. 2010; Smith et al. 2011; Oppenheimer et al. 2012). These studies have not explicitly examined the physical nature of the CGM for individual galaxies and likely have insufficient resolution to perform such analysis. A few authors have examined the distribution of gas within individual galactic haloes, but have not yet treated the distribution of metals or the impact of feedback (Kereš & Hernquist 2009; Stewart et al. 2011). At $z \sim 3$, Kawata & Rauch (2007) have analysed numerical simulations of outflows in $L^\star$ progenitors and found that O VI better reflects the strength of galactic winds than H I. Most recently, Fumagalli et al. (2011) and Shen et al. (2011) have examined the metal enrichment of the CGM with the latter demonstrating that metals can be ejected to large distances at early times from $L^\star$ progenitor galaxies while their gravitational potential remains low.

We have recently begun the Making Galaxies In a Cosmological Context (MAGICC) project to use sufficient stellar feedback to simulate galaxies that match the stellar mass–halo mass relationship. Early results of the project have shown that the ejection of low angular momentum gas via outflows (Brook et al. 2011) redistributes angular momentum via large-scale galactic fountains (Brook et al. 2012a) and thus play a crucial role in forming disc galaxies, particularly those without classical bulges. In this way, we form galaxies that match scaling relations between rotation velocity, size, luminosity, colour, stellar mass, halo mass, H I mass, baryonic mass and metallicity (Brook et al. 2012b). Macciò et al. (2012) also showed that these galaxies have cored dark matter density profiles. Here, we test the baryon cycle of these simulations with the constraints provided by observations of the CGM, and in particular the column densities of H I and O VI as observed at $z = 0$.

2 SIMULATIONS

We resimulate a suite of simulations drawn from the McMaster Unbiased Galaxy Simulations (MUGS; Stinson et al. 2010). The simulations are listed in Table 1. The highest mass galaxy, HM, is g5664 from MUGS and is about half the Milky Way halo mass. The low-mass (LM) galaxies, LM_MF and LM_LF, are rescaled versions of MUGS initial conditions, each a factor of 8 lower mass than the MUGS, allowing us to explore mass dependence. LM_MF was also used in Brook et al. (2012a).

The simulations were evolved using the smoothed particle hydrodynamics (SPH) code GASOLINE (Wadsley et al. 2004). Supernova energy is implemented using the blast-wave formalism (Stinson

Table 1. Simulation data.

Name	M_{tot}[a] (M$_\odot$)	$M_\star$[b] (M$_\odot$)	Luminosity[c] ($L^\star$)	$c_\star$[d]	ϵ_{rp}[e]	IMF[f]
HM_MF	7×10^{11}	1.4×10^{10}	0.84	0.1	0.175	C
HM_LF	7×10^{11}	4.8×10^{10}	0.79	0.05	–	K
LM_MF	1.8×10^{11}	3.7×10^9	0.15	0.05	0.1	C
LM_LF	8.8×10^{10}	8.7×10^9	0.13	0.05	–	K

[a]M_{tot} is the virial mass of the halo including dark and baryonic matter.
[b]$M_\star$ is the total stellar mass.
[c] V-band luminosity compared to $M_V = -21$.
[d]Star-forming efficiency.
[e]Radiation pressure efficiency.
[f] Initial mass function: C = Chabrier (2003); K = Kroupa, Tout & Gilmore (1993).

et al. 2006). Metals are ejected from Type II supernovae, Type Ia supernovae and the stellar winds of asymptotic giant branch stars. Ejected mass and metals are distributed to the nearest-neighbour gas particles using the smoothing kernel (Stinson et al. 2006). Metal diffusion is included, and metal cooling is calculated based on the diffused metals (Shen, Wadsley & Stinson 2010).

Two different star formation and feedback models are employed. The original MUGS formed stars when gas reached a density of $1.0\,cm^{-3}$, used a Kroupa et al. (1993) initial mass function (IMF) and deposited 0.4×10^{51} ergs per supernova explosion. We refer to this as the 'lower feedback (LF) model' in this study, but note that this feedback strength is comparable to or even stronger than most implementations that are currently run in the literature (Scannapieco et al. 2012). In our 'MAGICC feedback (MF) model', four changes have been made to our implementation of star formation and feedback:

(i) we use the more common Chabrier (2003) IMF which creates more massive stars for a given stellar mass;

(ii) the star formation density threshold is increased to $9.3\,cm^{-3}$;

(iii) the energy input from supernovae is increased to 10^{51} ergs;

(iv) we include energy from radiation released by the massive young stars before they explode as supernovae.

Radiation pressure from massive stars can have significant effects on the scales that are resolved in our simulations (Nath & Silk 2009; Murray, Ménard & Thompson 2011). Massive stars typically produce 10^{50} ergs of energy per $M_\odot$, yet this couples only weakly to the interstellar medium (ISM; Freyer, Hensler & Yorke 2006). To mimic this inefficiency, we inject a fraction of the energy as thermal energy in the surrounding gas but do *not* turn off cooling (for details see Brook et al. 2012a). Such thermal energy injection is highly inefficient at the spatial and temporal resolution of cosmological simulations and is rapidly radiated away (Katz 1992). This feedback is even less efficient at low resolution. Following a parameter search designed to match the stellar mass–halo mass resolution from halo abundance matching (Moster et al. 2010), we inject 17.5 per cent of radiation pressure to the surrounding gas as thermal energy in the lower resolution (HM) simulation, but only 10 per cent in the higher resolution runs (LM). The overall coupling of energy to the ISM is minimal, but sufficient to reduce star formation in the region immediately surrounding a recently formed star particle.

The HM_LF and HM_MF simulations use the same initial conditions, and each simulated galaxy has an absolute V-band magnitude $M_V \approx -20.8$ implying a luminosity $L \approx 0.8L^\star$. This is somewhat surprising given that the two runs yield very different stellar masses for the galaxy; this difference is compensated by the fact that each galaxy follows a very different star formation history (see Fig. 7) such that the different stellar ages result in comparable V-band luminosity, but $B - V$ colours of 0.37 for HM_MF and 0.55 for HM_LF. HM_MF was analysed in Macciò et al. (2012). LM_LF and LM_MF use different initial conditions of similar halo mass. They are selected because each has $M_V \approx -19$. The LM_LF initial conditions run with MF have $M_V \approx -16.2$. To summarize the internal properties of the galaxies, the LF galaxies suffer from the problems of angular momentum loss that have long plagued galaxy formation simulations: dense central stellar bulges, centrally peaked rotation curves, dark matter cusps and too many stars relative to halo mass compared to observations. The MF simulations result in galaxies which match the stellar mass–halo mass relation, and have slowly rising rotation curves and dark matter cores. The MF simulations provide significantly better matches to the internal properties of observed disc galaxies.

3 RESULTS

To study the CGM properties of the simulated galaxies, we find the galaxy using the AMIGA Halo Finder (Knollmann & Knebe 2009) and define its centre and systemic velocity by the position and velocity of the particle with the lowest potential. We may then sample the CGM at a range of impact parameters ρ. To generate the surface density maps of the CGM, we sum each box over 1 Mpc along the line of sight. The maximum velocity of the material in the box is $|\delta v| < 200\,km\,s^{-1}$. To estimate the specific column densities of H I and O VI, we must estimate the ionization state of the gas along each sightline. Under equilibrium conditions, which we assume to apply, the ionization state is determined by the incident radiation field (photoionization) and temperature of the gas (collisional ionization). Proper handling of radiative transfer effects is beyond the scope of this paper. Instead, we examine the simulations in regions expected to correspond to optically thin material, i.e. where the H I column density is low because the gas is expected to be highly ionized.

We calculated the ionization states for hydrogen and oxygen throughout the high-resolution region assuming optically thin conditions and the Haardt & Madau (2012) ultraviolet radiation field evaluated at $z = 0$. With the CLOUDY software package (v10.0 last described in Ferland et al. 1998), we generated a suite of models varying the density, temperature and metallicity of the medium, and used the output to find the O VI and H I fractions for all the gas in the simulation.

In Fig. 1, we present column density maps for H I and O VI for the LF and MF runs of galaxy HM. Both simulations predict a CGM extending to at least 100 kpc traced by cool H I gas and the more highly ionized O VI gas. Fig. 2 presents three phase diagrams of the CGM material in each galaxy. The top phase diagrams include the total halo gas mass in the simulations. The middle only counts H I mass and the bottom only counts the mass of the halo O VI. One notes two distinct phases in the top panels: (i) a cool ($T \sim 10^4$ K), dense ($n > 10^{-2}\,cm^{-3}$) gas which dominates the H I absorption and (ii) a warm/hot ($T > 10^5$ K) gas, which, as the bottom panels show, creates the O VI, primarily through collisional ionization.
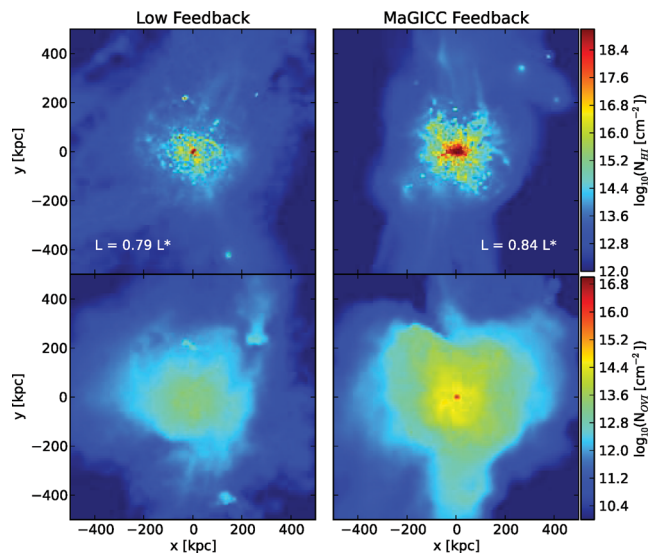

Figure 1. Column density maps of H I (top) and O VI (bottom) of the low (left) and high (right) feedback simulations. The maps are all aligned so that the discs of the galaxies are edge on to the viewer. The results on scales greater than 10 kpc are relatively independent of the viewing angle.
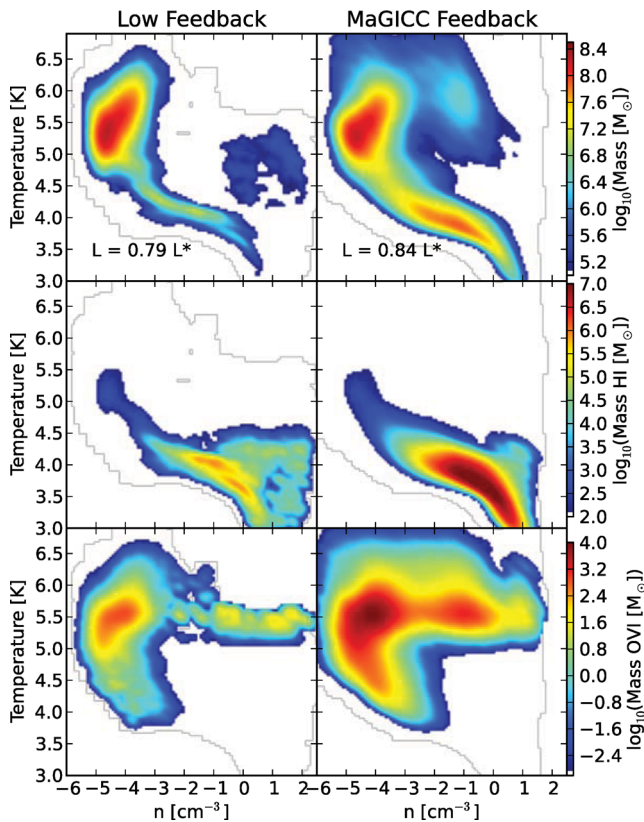
Figure 2. Temperature–density phase diagrams of the galaxy halo simulated with the two different amounts of feedback. The top plots are mass weighted by the total gas mass, the middle is weighted by the H I mass and the bottom is weighted by O VI. These phase diagrams only include halo gas, that is gas more than 3 kpc above or below the mid-plane or at $R_{xy} > 40$ kpc. The distinct locations of O VI and H I show that the hot and cold gases are in different phases in our model.

The MF simulation shows a high-density, hot component, which seems unphysical that accounts for 9 per cent of the halo O VI at $z = 0$. We find that 90 per cent of this high-density, hot halo gas is a relic of the thermal feedback implementation – the gas has had its cooling temporarily disabled – and that this gas is concentrated in an $\sim$10 kpc sphere around the galaxy. This dense, hot gas drives the outflows that populate the CGM with metal-enriched material, but it represents a negligible fraction of the O VI column. We discuss in Section 3.3 how this dense, hot gas generates a comparable amount of soft X-ray emission to that observed.

In terms of total mass, Fig. 3 shows that the CGM of the HM_MF galaxy has 4×10^{10} M$_\odot$ (7×10^{10} M$_\odot$) of gas to $\rho = 150$ (300) kpc. (We quote 300 kpc since it is the maximum extent at which O VI maintains a 100 per cent covering fraction in the simulations.) About half of this CGM has temperature $T < 10^5$ K giving a cool gas mass that matches very well with previous empirical estimates (Prochaska et al. 2011b). Regarding metals, the CGM has $\sim$10^6 M$_\odot$ of O VI to $R = 150$ kpc, again in excellent agreement with the mass estimates for $L \approx L^\star$ star-forming galaxies (Tumlinson et al. 2011). The LM_MF model has a lower CGM mass in both gas and metals by about a factor of 3. The LM_LF has even less ($\sim$10^9 M$_\odot$) cool gas in the CGM and a negligible mass of O VI. This model is a very poor match to the observational estimates.

Returning to Fig. 1, one notes that the O VI gas has both a smoother and more extended distribution than the H I. Again, this reflects the fact that the O VI gas traces a hotter and more diffuse phase in
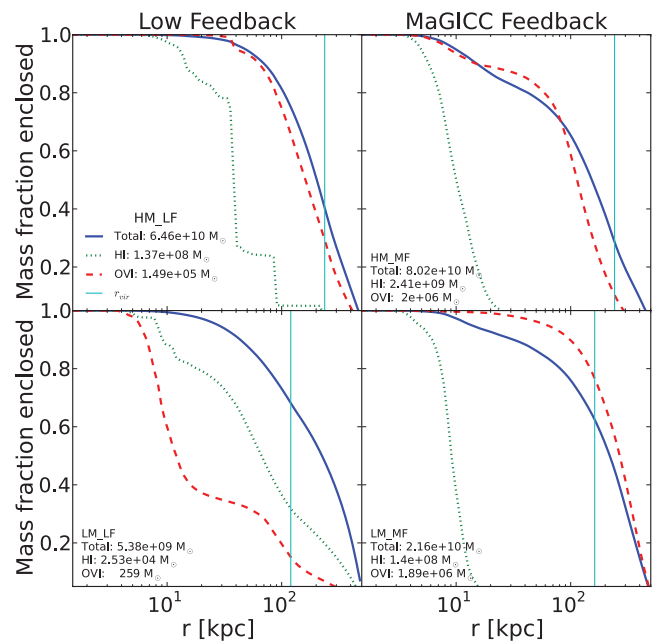
Figure 3. Cumulative gas mass profiles from 500 kpc inwards for each of the four galaxies. The solid line represents total gas mass, the dashed line represents O VI and the dotted line represents H I. The total mass of each component is given in the legend of each plot. With the MF, the H I has a more centrally concentrated profile than the O VI. In the $\sim L^\star$ galaxy, HM_MF, the O VI distribution follows the total gas distribution fairly closely, but in the lower mass galaxy, the O VI is significantly more extended than the total gas, indicating that enriched material is blown farther away.

the haloes of this galaxy. In contrast, the discrete clouds of H I are clustered more closely to the disc and are the remnants of gas-rich mergers, cooling out of the hot halo. Maller & Bullock (2004) and Kaufmann et al. (2009) describe how gas can cool out of the hot halo. A detailed examination of the evolution of these cold clouds is beyond the scope of this paper, but a preliminary investigation suggests that the clouds both cool out of the hot halo and are entrained in the outflows. The cooling mechanism may be a numerical artefact of SPH whereby particles approach each other due to random excursions and thus create a slightly higher density, which makes them cool faster. Fewer condensations are seen using hydrodynamics based on the Eulerian (grid) method (Teyssier 2002; Agertz, Teyssier & Moore 2011) or the new moving mesh code AREPO (Springel 2010; Vogelsberger et al. 2011). It remains for future simulations, using more detailed radiative transfer, to see if such condensations are an artefact of the SPH scheme.

In Fig. 4, we present the surface density profiles of H I gas and in Fig. 5 those of O VI gas as a function of the impact parameter ρ to the centre of the galaxy. Overplotted on the distributions are observed H I and O VI column densities for sub-$L^\star$ galaxies at $z \sim 0$ from Prochaska et al. (2011a) and for star-forming $L^\star$ galaxies at $z \sim$ 0.2 from Tumlinson et al. (2011). We also mark each panel with the V-band luminosity of the simulated galaxies and the virial radius, indicated by the vertical green line. Considering first the lower feedback HM_LF, we find fair agreement for the H I gas although the data are systematically higher than the majority of simulated sight-lines. The results for O VI are more discordant; the CGM of HM_LF underpredicts the observed O VI column densities by nearly an order of magnitude at all impact parameters. In contrast, the HM_MF predicts nearly 10 times higher O VI surface densities and therefore provides a reasonable match to the observations. Furthermore,
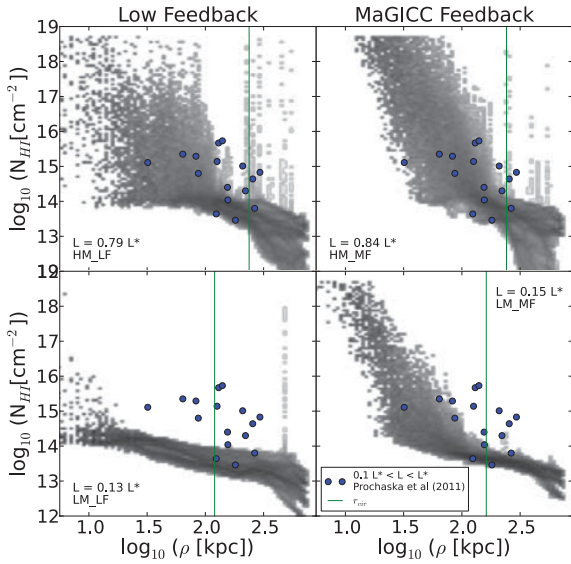
Figure 4. Radial profiles of the column density maps of H I for the four simulated galaxies. The large blue dots represent observations of $0.1 L^\star < L < L^\star$ from the Prochaska et al. (2011a) galaxy sample, while the large green squares galaxies with $L < 0.1 L^\star$. The solid green line represents the virial radius, $r_{\rm vir}$, for each of the four haloes.
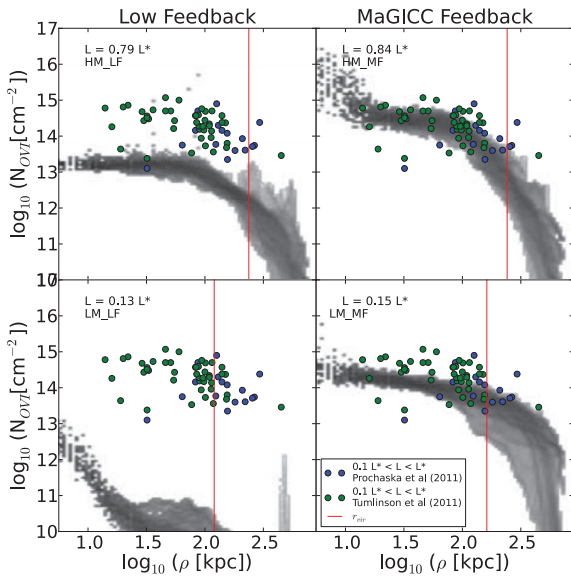

Figure 5. Radial profiles of the column density maps of O VI for four galaxies spanning a range of masses simulated using MF simulations. The large dots represent observations of $0.1 L^\star < L < L^\star$ galaxies from the Prochaska et al. (2011a) (blue) and Tumlinson et al. (2011) (green) galaxy samples. The solid red line represents the virial radius, $r_{\rm vir}$, for each of the four haloes.

this model yields qualitatively better agreement with the H I observations. In these respects, this single simulation of an $L \approx 0.8L^\star$ galaxy has a CGM with characteristics matching current observations. At lower masses, the differences between the high and lower feedback models become starker. LM_LF has an undetectable O VI content beyond the optical extent of the galaxy even though all the data for galaxies of comparable luminosity show detections of O VI. In contrast, LM_MF predicts a factor of 10^4 higher O VI surface densities, matching the observations.

3.1 Halo oxygen distribution function

Fig. 6 shows the oxygen distribution function of the halo gas in the four simulations. The MF cases result in a broad distribution of oxygen abundance with a peak at half the solar oxygen abundance comparable to the abundances measured in the Milky Way halo gas (Gibson et al. 2000, 2001). The LF simulations are at least two orders of magnitude less oxygen enriched. In total, HM_MF has $1.2 \times 10^8 \, {\rm M_\odot}$ of oxygen in its halo, roughly twice the $7.7 \times 10^7 \, {\rm M_\odot}$ of oxygen contained in the ISM in the disc, while LM_MF has roughly an equipartition between $1.6 \times 10^7 \, {\rm M_\odot}$ in its halo and $2.1 \times 10^7 \, {\rm M_\odot}$ in its disc (cf. Tumlinson et al. 2011). LF generates gaseous haloes with significantly less oxygen.

3.2 Evolution

To gain a sense of how the CGM developed, Fig. 7 shows the evolution of total mass, along with stellar, O VI, cold ($T < 10^5$ K) and hot
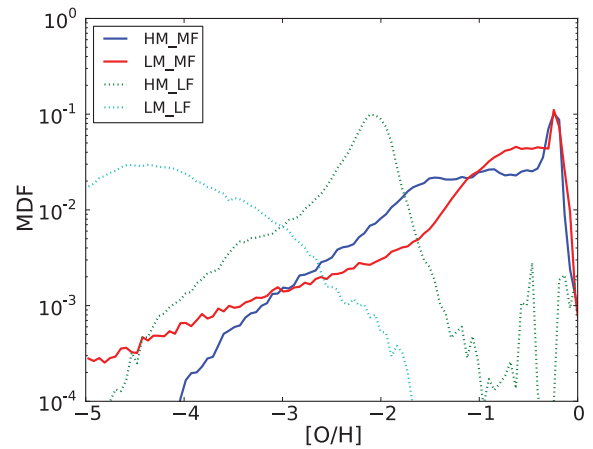

Figure 6. The oxygen distribution function for the four galaxies in our sample. The MF produces a significantly metal-enriched gas halo with a peak in both the HM and LM galaxies just above half-solar.
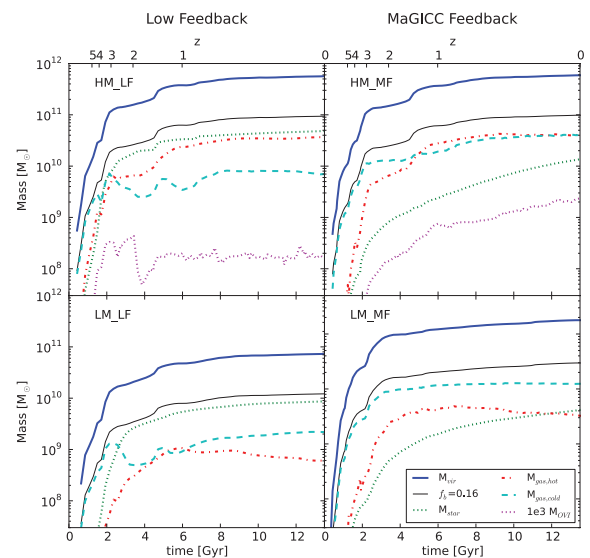

Figure 7. The mass evolution of the total halo mass (blue), stellar mass (dotted-green), $10^3 \times$ O VI mass (dotted-magenta), total gas (dashed light blue) and hot ($T > 10^5$ K) gas within $r_{\rm vir}$ for the four simulations. The thin black line shows the cosmic baryon fraction of the total halo mass.

gas ($T > 10^5$ K) masses within r_{vir} for the simulated galaxies. The total halo mass increases by two orders of magnitude in the 2 Gyr between $z = 6$ and 3 in each simulation. Subsequent merger/accretion events are reflected in mass 'jumps'. With LF, most star formation happens early; at the same time the total mass rapidly increases. High feedback delays this star formation.

In each galaxy, hot gas develops at the same time as star formation, indicating that stellar feedback is the initial source of hot gas in galaxy haloes. As the halo grows, accreting cold gas is shocked to the virial temperature, so that by $z = 0$, only one third of $T > 10^5$ K gas at $z = 0$ was directly involved in a stellar feedback event. The mass history of the O VI follows stellar mass in HM_MF indicating that oxygen produced in supernovae readily makes its way into the halo as a hot gas. In HM_LF, the O VI mass initially rises, but then drops during its major merger at $z = 1.5$ after which the O VI mass remains constant indicating that the LF is unable to drive metal-enriched outflows.

It is surprising that even though the feedback implementation is thermal, the MF does not lead to more hot gas, but rather more cold gas. As described earlier, this is because some cold gas gets entrained in outflows and there is rapid cooling of halo gas. We speculate that the similar amount of hot gas in HM_LF and HM_MF that have different feedback implementations is representative of some maximum amount of hot gas that can exist in a halo before the gas cools; a larger parameter search is required to address this question.

3.3 X-ray emission

One consequence of predicting that the O VI comes from a massive halo of collisionally excited gas ranging up to 10^7 K is that it should produce diffuse soft (0.2–2.0 keV) X-ray emission. Observations of disc galaxies have detected X-rays from outflows less than 10 kpc from the disc, but never $L_X > 5.2 \times 10^{39}$ erg s^{-1} outside 10 kpc (Strickland et al. 2004; Anderson & Bregman 2011). Using a naive Navarro, Frenk & White (1995) estimate of L_X based solely on bremsstrahlung cooling, HM_MF has $L_X = 5.2 \times 10^{39}$ (4.4 × 10^{37}) erg s^{-1} outside 10 (20) kpc in the 0.2–2.0 keV energy range. Even with the large amount of mass in the halo, the gas remains too diffuse to emit significant X-rays. It is intriguing that the X-ray luminosity from inside 10 kpc, $L_X = 5.8 \times 10^{40}$, is similar to the observed diffuse, soft X-ray emission for an $L_B = 2.4 \times 10^{10}$ L$_\odot$ galaxy (e.g. Strickland et al. 2004), but a detailed study of this emission is beyond the scope of this work.

4 CONCLUSIONS

We have studied CGM gas in high-resolution galaxy formation simulations. The stellar feedback is constrained using the stellar mass–halo mass relationship. This constraint leads to a stellar feedback implementation that decreases star formation and ejects hot, metal-enriched gas into the CGM. Inside the galaxies, the stellar feedback results in slowly rising rotation curves, flattened dark matter density profiles and H I mass–luminosity, baryonic Tully–Fisher relations, and mass–metallicity relations that resemble observed galaxies (Brook et al. 2012b). We compared these galaxy models to one with more standard feedback implementation (Stinson et al. 2010; Scannapieco et al. 2012). The LF simulations match none of these commonly observed internal properties of galaxies. An examination of the CGM in our model reveals the following.

(i) The MF implementation produces extended, metal-enriched gaseous coronae that extend to impact parameters of ∼300 kpc, even around low-mass ($L^\star \sim 0.1$ L$_\odot$) haloes. These results match observed absorption-line features (Wakker & Savage 2009; Prochaska et al. 2011b; Tumlinson et al. 2011).

(ii) The hot coronae extend beyond r_{vir}, though most of their mass remains contained within r_{vir} of the simulated galaxies. The coronae extend furthest outside r_{vir} in low-mass systems.

(iii) A reasonably strong feedback implementation, compared with those in the literature (our 'LF' case), is insufficient to match H I absorption features at $z = 0$ and severely underestimates O VI, performing particularly poorly in low-mass (∼0.1 $L^\star$) simulations.

(iv) The amount of hot gas in the LF and MF runs did not differ significantly, but rather

(a) the MF ejected 10 times more oxygen out of the disc than the LF in the high-mass case and a factor of 10^4 more in the low-mass case;

(b) the MF halo contains 10 times the cold gas as the LF case in both high- and low-mass simulations. The cold gas results from cooling out of the hot halo gas and cold gas entrained in outflows.

(v) The MF simulations match the observed H I and O VI absorption columns at a range of masses.

(vi) The total mass of the coronae is several times higher than the stellar mass in the simulated MF galaxies. Thus, the simulations of individual galaxies predict that the 'missing baryons' are found in the CGM of galaxies.

In our simulations, we only considered galaxies defined as star forming by Prochaska et al. (2011a) and Tumlinson et al. (2011). One of the key results of those works is the absence of O VI detection in quiescent galaxies. Our simulations are unable to address the question of what happens to the O VI when galaxies stop forming stars.

Our examination focused on the radial distribution of H I and O VI gas in the CGM of a simulated $L \approx L^\star$ galaxy and compared these results to observed surface density profiles. There are, of course, additional observables related to the entire population of O VI absorbers identified in quasar absorption-line studies (e.g. Danforth & Shull 2008; Thom & Chen 2008a; Tripp et al. 2008); any truly successful model must also reproduce these results. One key constraint is the observed distribution of line widths (also known as Doppler parameters or b values) for the O VI gas (Thom & Chen 2008a; Tripp et al. 2008) which gauge, in a statistical fashion, the contributions of thermal broadening, turbulence and gas dynamics to the motions of the gas. On average, the b values for O VI absorbers are substantial ($b > 20$ km s^{-1}) and appear to correlate with the strength of O VI absorption. This has posed a considerable challenge to models where O VI is predominantly photoionized (e.g. Oppenheimer & Davé 2009), as such gas has a small thermal width. Another valuable kinematic constraint is the common observation of co-aligned H I and O VI absorption relative to a common redshift (approximately half of observed O VI systems; Thom & Chen 2008b). Indeed, this appears to be at odds with the apparent separation of strong H I absorption (at smaller radii) with the extended O VI absorption of our modelled CGM. On the other hand, we do observe non-negligible H I absorption to large radii (Fig. 4) which may trace the O VI gas. A proper comparison of our model with these observables will require the generation and detailed analysis of line profiles, as well as the examination of the CGM for galaxies spanning a wide range of masses. This will be the focus of our next paper, which will consider whether the extended CGM of $z \sim 0$ galaxies can reproduce

all of the observed statistics for O VI as argued by Prochaska et al. (2011b).

We further note that the H I surface densities at $\rho < 50\,\mathrm{kpc}$ are sufficiently large that the CGM will yield significant absorption from lower ionization states of heavy metals (e.g. Mg II, Si II, Si III). A proper estimate of the column densities for these ions, however, will require a full treatment of radiative transfer (i.e. to account for self-shielding by optically thick H I gas).

The fact that the resultant extended, metal-enriched CGM around our simulated galaxies matches the observations over a wide range of mass provides strong support for a vigorous baryon cycle in which outflows and subsequent cooling of halo gas play a key role in forming disc galaxies.

ACKNOWLEDGMENTS

REFERENCES

Agertz O., Teyssier R., Moore B., 2011, MNRAS, 410, 1391
Allen S. W., Schmidt R. W., Fabian A. C., 2001, MNRAS, 328, L37
Anderson M. E., Bregman J. N., 2011, ApJ, 737, 22
Barton E. J., Cooke J., 2009, AJ, 138, 1817
Binney J., Nipoti C., Fraternali F., 2009, MNRAS, 397, 1804
Bowen D. V., Blades J. C., Pettini M., 1996, ApJ, 464, 141
Brook C. B. et al., 2011, MNRAS, 415, 1051
Brook C. B., Stinson G., Gibson B. K., Roškar R., Wadsley J., Quinn T., 2012a, MNRAS, 419, 771
Brook C. B., Stinson G., Gibson B. K., Wadsley J., Quinn T., 2012b, MNRAS, preprint (arXiv:e-prints)
Cen R., 2010, ApJ, 753, 17
Cen R., Ostriker J. P., 2006, ApJ, 650, 560
Chabrier G., 2003, PASP, 115, 763
Chen H.-W., Lanzetta K. M., 2003, ApJ, 597, 706
Chen H.-W., Tinker J. L., 2008, ApJ, 687, 745
Conroy C., Wechsler R. H., 2009, ApJ, 696, 620
Danforth C. W., Shull J. M., 2008, ApJ, 679, 194
Davé R., Oppenheimer B. D., Katz N., Kollmeier J. A., Weinberg D. H., 2010, MNRAS, 408, 2051
Ferland G. J., Korista K. T., Verner D. A., Ferguson J. W., Kingdon J. B., Verner E. M., 1998, PASP, 110, 761
Freyer T., Hensler G., Yorke H. W., 2006, ApJ, 638, 262
Fumagalli M., Prochaska J. X., Kasen D., Dekel A., Ceverino D., Primack J. R., 2011, MNRAS, 418, 1796
Gibson B. K., Giroux M. L., Penton S. V., Putman M. E., Stocke J. T., Shull J. M., 2000, AJ, 120, 1830
Gibson B. K., Giroux M. L., Penton S. V., Stocke J. T., Shull J. M., Tumlinson J., 2001, AJ, 122, 3280
Guo Q., White S., Li C., Boylan-Kolchin M., 2010, MNRAS, 404, 1111
Guo Q. et al., 2011, MNRAS, 413, 101
Haardt F., Madau P., 2012, ApJ, 746, 125
Katz N., 1992, ApJ, 391, 502
Kaufmann T., Bullock J. S., Maller A. H., Fang T., Wadsley J., 2009, MNRAS, 396, 191
Kawata D., Rauch M., 2007, ApJ, 663, 38
Kereš D., Hernquist L., 2009, ApJ, 700, L1
Knollmann S. R., Knebe A., 2009, ApJS, 182, 608
Kroupa P., Tout C. A., Gilmore G., 1993, MNRAS, 262, 545
Lanzetta K. M., Wolfe A. M., Turnshek D. A., 1995, ApJ, 440, 435
Macciò A. V., Stinson G., Brook C. B., Wadsley J., Couchman H. M. P., Shen S., Gibson B. K., Quinn T., 2012, ApJ, 744, L9
Maller A. H., Bullock J. S., 2004, MNRAS, 355, 694
Mandelbaum R., Li C., Kauffmann G., White S. D. M., 2009, MNRAS, 393, 377
Mo H. J., Miralda Escude J., 1996, ApJ, 469, 589
More S., van den Bosch F. C., Cacciato M., Skibba R., Mo H. J., Yang X., 2011, MNRAS, 410, 210
Moster B. P., Somerville R. S., Maulbetsch C., van den Bosch F. C., Macciò A. V., Naab T., Oser L., 2010, ApJ, 710, 903
Murray N., Ménard B., Thompson T. A., 2011, ApJ, 735, 66
Nath B. B., Silk J., 2009, MNRAS, 396, L90
Navarro J. F., Frenk C. S., White S. D. M., 1995, MNRAS, 275, 720
Oppenheimer B. D., Davé R., 2009, MNRAS, 395, 1875
Oppenheimer B. D., Davé R., Katz N., Kollmeier J. A., Weinberg D. H., 2012, MNRAS, 420, 829
Prochaska J. X., Weiner B., Chen H.-W., Mulchaey J., Cooksey K., 2011b, ApJ, 740, 91
Rubin K. H. R., Prochaska J. X., Koo D. C., Phillips A. C., Weiner B. J., 2010, ApJ, 712, 574
Rubin K. H. R., Weiner B. J., Koo D. C., Martin C. L., Prochaska J. X., Coil A. L., Newman J. A., 2010, ApJ, 719, 1503
Rubin K. H. R., Prochaska J. X., Koo D. C., Phillips A. C., 2012, ApJL, 747, 26
Savage B. D., Lehner N., Narayanan A., 2011a, ApJ, 743, 180
Savage B. D., Narayanan A., Lehner N., Wakker B. P., 2011b, ApJ, 731, 14
Scannapieco C. et al., 2012, MNRAS, 423, 726
Sembach K. R. et al., 2003, ApJS, 146, 165
Shapley A. E., Steidel C. C., Pettini M., Adelberger K. L., 2003, ApJ, 588, 65
Shen S., Wadsley J., Stinson G., 2010, MNRAS, 407, 1581
Shen S., Madau P., Aguirre A., Guedes J., Mayer L., Wadsley J., 2011, preprint (arXiv:1109.3713)
Smith B. D., Hallman E. J., Shull J. M., O'Shea B. W., 2011, ApJ, 731, 6
Springel V., 2010, MNRAS, 401, 791
Steidel C. C., Erb D. K., Shapley A. E., Pettini M., Reddy N., Bogosavljević M., Rudie G. C., Rakic O., 2010, ApJ, 717, 289
Stewart K. R., Kaufmann T., Bullock J. S., Barton E. J., Maller A. H., Diemand J., Wadsley J., 2011, ApJ, 738, 39
Stinson G., Seth A., Katz N., Wadsley J., Governato F., Quinn T., 2006, MNRAS, 373, 1074
Stinson G. S., Bailin J., Couchman H., Wadsley J., Shen S., Nickerson S., Brook C., Quinn T., 2010, MNRAS, 408, 812
Stocke J. T., Penton S. V., Danforth C. W., Shull J. M., Tumlinson J., McLin K. M., 2006, ApJ, 641, 217
Strickland D. K., Heckman T. M., Colbert E. J. M., Hoopes C. G., Weaver K. A., 2004, ApJ, 606, 829
Telfer R. C., Kriss G. A., Zheng W., Davidsen A. F., Tytler D., 2002, ApJ, 579, 500
Teyssier R., 2002, A&A, 385, 337
Thom C., Chen H.-W., 2008a, ApJS, 179, 37
Thom C., Chen H.-W., 2008b, ApJ, 683, 22
Thom C., Putman M. E., Gibson B. K., Christlieb N., Flynn C., Beers T. C., Wilhelm R., Lee Y. S., 2006, ApJ, 638, L97

Tripp T. M., Sembach K. R., Bowen D. V., Savage B. D., Jenkins E. B., Lehner N., Richter P., 2008, ApJS, 177, 39

Tumlinson J. et al., 2011, Science, 334, 948

Vogelsberger M., Sijacki D., Keres D., Springel V., Hernquist L., 2011, preprint (arXiv:1109.1281)

Wakker B. P., Savage B. D., 2009, ApJS, 182, 378

Wakker B. P., van Woerden H., 1997, ARA&A, 35, 217

Wakker B. P., Savage B. D., Fox A. J., Benjamin R. A., 2012, ApJ, 749, 157

Wedsley J. W., Stadel J., Quinn T., 2004, New Astronomy, 9, 127

Weiner B. J. et al., 2009, ApJ, 692, 187

This paper has been typeset from a TEX/LATEX file prepared by the author.